Environmental Toxicology and Chemistry—Volume 00, Number 00—pp. 1–14, 2021
Received: 16 September 2020 | Revised: 28 October 2020 | Accepted: 19 February 2021

Environmental Chemistry

Tackling the Challenge of Extracting Microplastics from Soils: A Protocol to Purify Soil Samples for Spectroscopic Analysis

Julia N. Möller,[a,*] Ingrid Heisel,[a] Anna Satzger,[a] Eva C. Vizsolyi,[a] S.D. Jakob Oster,[a] Seema Agarwal,[b] Christian Laforsch,[a,*] and Martin G.J. Löder[a,*]

[a]Department of Animal Ecology I and BayCEER, University of Bayreuth, Bayreuth, Germany
[b]Department of Macromolecular Chemistry II, University of Bayreuth, Bayreuth, Germany

Abstract: Microplastic pollution in soils is an emerging topic in the scientific community, with researchers striving to determine the occurrence and the impact of microplastics on soil health, ecology, and functionality. However, information on the microplastic contamination of soils is limited because of a lack of suitable analytical methods. Because micro-Fourier-transform infrared spectroscopy (μ-FTIR), next to Raman spectroscopy, is one of the few methods that allows the determination of the number, polymer type, shape, and size of microplastic particles, the present study addresses the challenge of purifying soil samples sufficiently to allow a subsequent μ-FTIR analysis. A combination of freeze-drying, sieving, density separation, and a sequential enzymatic-oxidative digestion protocol enables removal of the mineral mass (>99.9% dry wt) and an average reduction of 77% dry weight of the remaining organic fraction. In addition to visual integrity, attenuated total reflectance FTIR, gel permeation chromatography, and differential scanning calorimetry showed that polyamide, polyethylene, polyethylene terephthalate, and polyvinyl chloride in the size range of 100 to 400 μm were not affected by the approach. However, biodegradable polylactic acid showed visible signs of degradation and reduced molecular weight distribution after protease treatment. Nevertheless, the presented purification protocol is a reliable and robust method to purify relatively large soil samples of approximately 250 g dry weight for spectroscopic analysis in microplastic research and has been shown to recover various microplastic fibers and fragments down to a size of 10 μm from natural soil samples. *Environ Toxicol Chem* 2021;00:1–14. © 2021 The Authors. *Environmental Toxicology and Chemistry* published by Wiley Periodicals LLC on behalf of SETAC.

Keywords: Microplastics; Soil contamination; Analytical chemistry; Purification protocol; Enzymatic-oxidative digestion; μ-FTIR

INTRODUCTION

Introduction of macro- as well as microplastics into soils is estimated to exceed the numbers emitted into water bodies by far (Kawecki and Nowack 2019). Hence, a substantial proportion of plastic pollution is expected to enter and remain permanently in the soil column (Rillig et al. 2017; Hurley and Nizzetto 2018; Rochman 2018). One entryway for microplastics into soils is mismanagement of waste (Lebreton and Andrady 2019), but also common agricultural practices are known to introduce microplastics directly into soil systems, such as using treated wastewater for irrigation (He et al. 2018), applying sewage sludge and certain compost types as fertilizers (Weithmann et al. 2018; Corradini et al. 2019; Van den Berg et al. 2020), or practicing plastic-film mulching (Zhou et al. 2019). However, nonagricultural soils have also been shown to contain microplastics, such as floodplain soils (Scheurer and Bigalke 2018), soils on industrial sites (Fuller and Gautam 2016), and soils in home gardens (Huerta Lwanga et al. 2017).

Ongoing research indicates that different types of microplastics may potentially influence a soil's health and functionality in different ways. For instance, De Souza Machado et al. (2019) conducted a study in which soils and spring onions were exposed to 6 microplastic types, including beads, fibers, and fragments. The exposure experiments resulted in altered physical soil parameters as well as changes in plant performance. Treatments with polyamide (PA) beads and polyester fibers elicited the largest differences from the control treatments,

This article contains online-only Supplemental Data.

* Address correspondence to julia.moeller@uni-bayreuth.de, christian.laforsch@uni-bayreuth.de, martin.loeder@uni-bayreuth.de
Published online 23 February 2021 in Wiley Online Library (wileyonlinelibrary.com).
DOI: 10.1002/etc.5024

allowing the tentative assumption that the microplastic's shape and size may also be relevant to the impact on soil properties. To better assess the impact of plastics on soil functionality, it is indispensable to accurately evaluate the microplastic contamination with regard to polymer type, shape, and size. Therefore, appropriate analytical tools and methods are necessary.

To date, there is no established standard method for the sampling, extraction, purification, and identification/quantification of microplastic particles in soil samples (Möller et al. 2020). However, methods developed for analyzing aquatic sediments, which have been the focus of research for a comparatively longer time than soils, can potentially be adapted and the lessons learned from them considered for the processing of soil samples for microplastic analysis. The following paragraph describes several methods mentioned in the literature to extract microplastics from sediment and soil samples.

One of the simplest methods used to extract microplastic particles from soil samples is manual sorting, which is often applied for particles >1 mm (Piehl et al. 2018, soil). Other methods used are oil extraction (Scopetani et al. 2020, compost and soil) and density separation with highly dense salt solutions using NaI, $ZnCl_2$, NaBr, or $Na_6[H_2W_{12}O_6]$ (Möller et al. 2020, diverse matrices) to remove the mineral matrix. These extraction procedures are often found in combination with one or several purification steps to remove the organic components. These can include an oxidization step with hydrogen peroxide (H_2O_2; Nuelle et al. 2014, marine sediment) or Fenton's reagent (Tagg et al. 2017, wastewater; Hurley et al. 2018, sludge and soil) or alternatively an enzymatic digestion procedure (Löder et al. 2017, marine sediment and water). The methodologies used to identify the microplastic particles also vary between microplastic research groups. Some methods are based on visual identification, for example, by staining the microplastic particles with the fluorescent Nile red (Maes et al. 2017, marine sediment), while others rely on a combination of gas chromatography and mass spectrometry (GC-MS) to identify the polymer type and mass of the microplastics in a sample. Examples of this type of approach include pyrolysis GC-MS used for marine sediments (Nuelle et al. 2014) and thermal extraction desorption (TED) GC-MS developed by Dümichen et al. (2017) and used for digestate. These methods, however, only allow the analysis of very small sample sizes (0.5 mg for pyrolysis GC-MS and 20 mg for TED GC-MS), and therefore require a high degree of sample purification if a larger amount of sample is targeted (Dümichen et al. 2017). It is also important to note the loss of information on particle numbers, sizes, and shapes when using these methods. In comparison, focal plane array (FPA)–based micro-Fourier-transform infrared spectroscopy (μ-FTIR) and Raman microspectroscopy are established methods that can identify the polymer type, number, shape, and size of small (<500 μm) microplastic particles within environmental samples (Löder et al. 2015; Kumar et al. 2021). A precondition for the identification of microplastic particles via these methods is that microplastic particles are extracted and ideally isolated from the environmental matrix (Löder et al. 2017).

Opposed to aquatic sediments, soils are rich in terrestrial plant debris and humus, which are difficult to break down. Although harsh purification steps with, for example, strong acidic solutions are able to destroy the organic soil content, they also alter the original plastic composition by destroying labile plastic types (Scheurer and Bigalke 2018). To our knowledge, no plastic-conserving approach has been published yet that explicitly addresses those issues related to the spectroscopic analysis of microplastics (10 μm–5 mm) in soil samples. Therefore, we developed an effective sample purification protocol specifically for the extraction and purification of microplastics (10 μm–5 mm) from soil samples that allows removal of the bulk mineral matter via density separation and removal of the organic matter by a plastic-friendly enzymatic-oxidative digestion protocol, thereby conserving the original plastic composition.

We investigated the purification efficiency of the protocol for an agriculturally used silt loam soil by analyzing the mass reduction of the total purification protocol. To validate the plastic-friendliness, potential destructive effects on microplastics sized 100 to 400 μm of different plastic types—PA, polyethylene (PE), polyethylene terephthalate (PET), polyvinylchloride (PVC), and polylactic acid (PLA)—were analyzed. We investigated visual integrity and changes in the functional groups on the polymer surfaces via attenuated total reflectance (ATR)–FTIR spectroscopy, mean molar mass distribution via gel permeation chromatography (GPC), as well as changes in the thermal transition characteristics via differential scanning calorimetry (DSC).

MATERIALS AND METHODS

The protocol is designed to allow the extraction and identification of microplastics from 10 μm to 5 mm. Because the process of manual extraction and ATR-FTIR analysis of particles >500 μm is not new as such, the focus will mainly lie on the purification procedure for particles <500 μm. Empirical experiments concerning the purification efficiency were conducted using three 250-g subsamples of a composite sample of silt-loam soil obtained from the first 10 cm of an experimental agricultural field near Stuttgart, southwest Germany, on 4 December 2019. Another 250-g aliquot of the same soil was used to verify the purification method for analysis of a natural sample.

Prevention of sample contamination

Sample contamination with microplastic particles from the ambient air, clothing, chemicals, or laboratory tools is a significant concern in microplastic analysis of environmental samples. Thus, precautionary measures were applied. Samples were always covered with a glass lid or aluminum foil unless direct handling was necessary. In this case samples were handled under a laminar-flow box. The tools used were made of glass, metal, or polytetrafluorethylene (PTFE), which is excluded from analysis. All required reagents and deionized

water were filtered through 0.2-µm-pore membranes (0.2-µm mixed cellulose ester membrane, diameter 47 mm, Whatman ME 24; Merck) before use, and enzymes were filtered through 0.45-µm membranes (0.45-µm regenerated cellulose membrane, diameter 100 mm, Whatman RC 55; Merck). All laboratory equipment was thoroughly rinsed with prefiltered deionized water, 35% ethanol, and again water before use and in between steps. Screw caps made of plastics were replaced by glass caps. Cotton laboratory coats were worn at all times. Blank samples undergoing the same procedures as the environmental samples were used to monitor possible contamination.

Detailed description of the purification procedure

Following is a description of the purification procedure in a step-by-step manual. Figure 1 shows a flowchart of the entire process.

Sampling and subsampling. Depending on the research question, different soil sampling techniques may be required (Möller et al. 2020), but often the field-sample amount exceeds the 250 g that can be processed with this protocol. Therefore, homogenized (thoroughly mixed but not ground) soil samples (~2 kg) are divided into subsamples of 250 g by the cone-and-quarter method described by Schumacher et al. (1990).

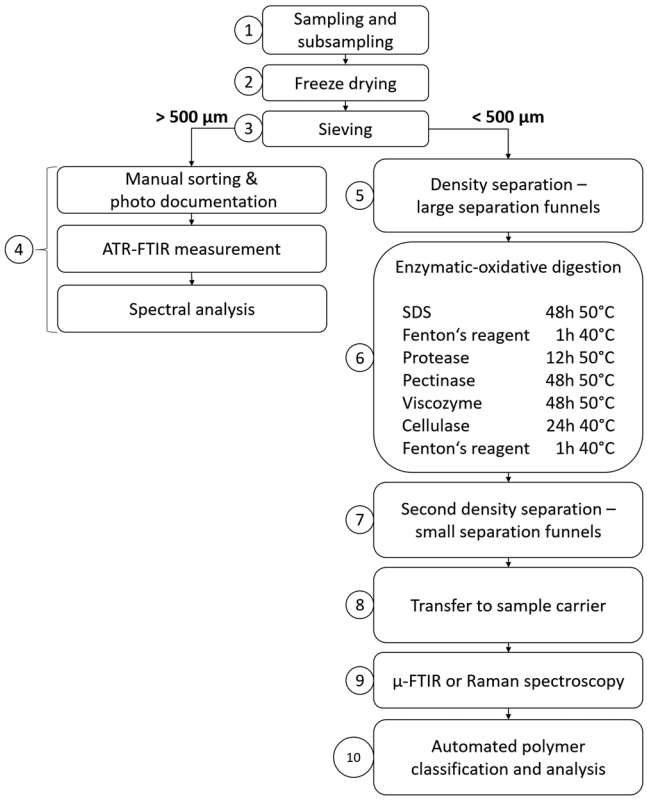

FIGURE 1: Flowchart of the soil purification protocol for microplastic analysis (10 µm–5 mm). ATR-FTIR = attenuated total reflectance Fourier-transform infrared spectroscopy; SDS = sodium dodecyl sulfate; µ-FTIR = micro-Fourier-transform infrared spectroscopy.

Freeze drying. Subsamples are freeze-dried under vacuum for 24 h to reduce the soil's aggregate stability (Staricka and Benoit 1995).

Sieving. Subsamples are wet-sieved with prefiltered (0.2 µm) deionized water through a sieve cascade with mesh sizes of 5 mm, 1 mm, and 500 µm (50 mm height, 203 mm diameter; Retsch).

Proceedings for particles >500 µm. The residues on the larger sieves (>500 µm) are manually sorted under a stereomicroscope with forceps, photographed, and stored for a subsequent ATR-FTIR measurement and spectral analysis of all potential microplastic particles (Löder et al. 2017).

Density separation for particles <500 µm. The suspension containing the <500-µm soil fraction is transferred into a precleaned, 2-L-volume glass beaker; covered with a glass lid; and left to settle overnight. This greatly facilitates decanting and filtering the supernatant water over stainless steel mesh filters (47 mm diameter, mesh size 10 µm; Rolf Körner; filtration unit 3-branch stainless steel vacuum manifold with 500-mL funnels and lids; Sartorius) to remove the water in preparation for a density separation step with a highly dense aqueous zinc chloride ($ZnCl_2$) solution ($\rho = 1.8\ g\ cm^{-3}$; Th. Geyer; Imhof et al. 2012). The filter is kept, and the retained particles are washed back into the beaker with the prefiltered (with a 1-µm polypropylene (PP) absolute filter cartridge, followed by a 2-µm stainless steel mesh filter) $ZnCl_2$ solution. If necessary, the particles may be scraped off the filter gently using a small metal spatula. The sludge remaining at the bottom of the beaker is then mixed with approximately 1 L of the prefiltered $ZnCl_2$ solution
and stirred with a stir bar for 20 to 30 min to disperse any remaining aggregates. Subsequently, a custom-made straight-walled glass separation funnel (Ø = 15 cm, H = 45 cm) with a volume capacity of approximately 4 L is filled with approximately 1 L $ZnCl_2$ solution, and an overhead stirrer (LLG-uniSTIRRER OH2, 3-hole paddle stirrer, Ø = 67 mm) is inserted and set to 50 rpm. Under continuous stirring, the homogenized soil–$ZnCl_2$ mixture is transferred into the separation funnel, and another 1 L of the $ZnCl_2$ solution is used to rinse all remaining particles from the beaker into the funnel, resulting in a final volume of approximately 3 L. The filled separation funnel is then covered with aluminum foil and stirred for 2 h before being left to settle overnight. After a minimum of 12 h of sedimentation, the bottom sediment and $ZnCl_2$ solution are slowly drained from the funnel, collected, and stored in a clean glass beaker, leaving the low-density fraction (i.e., organic and plastic) floating in the supernatant (0.6 L) in the separation funnel. This fraction is then discharged into a second clean glass beaker via the tap at the bottom and rinsed out of the separation funnel with a fresh $ZnCl_2$ solution. The collected supernatant is then filtered over 10-µm stainless steel mesh

filters. The filter cake is then briefly washed with 98% filtered (0.2 µm) ethanol and then with filtered deionized water to remove residual $ZnCl_2$. This filter cake is then placed, along with the filter, into a 290 mL precleaned mason jar with a glass lid (WECK) to be further processed with the sequential enzymatic-oxidative digestion protocol (see section *Enzymatic-oxidative digestion*).

The density separation procedure is then conducted a second time with the drained sediment, to increase recovery. The supernatant is collected and filtered, and the filter cake and second filter are added to the same mason jar as the supernatant collected from the first density separation because it is part of the same sample. The $ZnCl_2$ solution used during the density separation process is collected and regenerated by filtration for future use. The density of the $ZnCl_2$ solution is checked during regeneration, if the solution reaches a density of 1.7 g cm^{-3} as a result of the dilution with the moist sample, more $ZnCl_2$ is added to increase the density back to 1.8 g cm^{-3}.

Enzymatic-oxidative digestion. The present enzymatic purification protocol for soil samples is an optimized adaptation of the universal enzymatic purification protocol published by Löder et al. (2017).

The filter cake containing the low-density fraction of the density separation step is consecutively washed off the stainless steel filters into a reaction jar with a small amount of water or buffer using a self-designed high-pressure spray bottle with a needle nozzle, to which the respective chemical reagent or enzyme is added (see Table 1). The filters are also placed into the reaction jar. The mixture is then incubated at the respective temperature (see Table 1), under gentle agitation in an incubation cabinet. Subsequently, the filters, which are continuously used in every procedural step, are taken out of the jar and thoroughly rinsed with filtered, deionized water, washing any adhering particles back into the reaction jar. The cleaned filters are then placed into the stainless steel vacuum filtration unit funnels, through which the sample is then filtered. The jar is thoroughly rinsed onto the filters, and the filter cake on the stainless steel filters is washed with filtered deionized water to avoid reagents from the previous step interfering with subsequent reactions. Thereafter, any residual particles sticking to the filtration funnel are washed into the reaction jar with water or the appropriate buffer to avoid further dilution. The filters and filter cake are also added for the consecutive step.

Step a. Sodium dodecyl sulfate (SDS) is an anionic detergent capable of solubilizing lipids and proteins from cell walls (Ciccolini et al. 1998). We used 50 mL of a 10% (w/v) SDS solution per reaction jar, incubated for 48 h at 50 °C.

Step b. Fenton's reagent is a strong oxidizing agent composed of H_2O_2 and a ferrous ion (Fe^{2+}) catalyst, proposed in several previous publications as purification protocols for complex environmental samples because it is more effective at removing organic compounds than H_2O_2 alone (Tagg et al. 2017; Hurley et al. 2018). In the present protocol, 25 mL of 30% H_2O_2 is added to the sample and continuously stirred with a magnetic stir bar, before adding 25 mL of a 0.05 M Fe(II) solution (composed of 7.5 g iron[II] sulfate heptahydrate [$FeSO_4 \times 7H_2O$] in 500 mL ultrapure water and 3 mL concentrated sulfuric acid). The reaction with organic compounds is strongly exothermic; thus, an ice bath should be made ready beforehand and used when the reaction temperature reaches 38 to 39 °C to keep the reaction temperature below 40 °C because too high temperatures may adversely affect some microplastic particle types (Munno et al. 2018).

Step c. Protease hydrolyzes insoluble protein structures into soluble peptides. In the present study, 5 mL of Protease A-01 (subtilisin, EC 3.4.21.62, enzymatic activity 1.100 U mL^{-1}; ASA Spezialenzyme) are used in 25 mL of 0.1 M Tris-HCl buffer, set to pH 9.0 with concentrated HCl. The samples are then incubated at 50 °C for 12 h.

Step d. Dead plant matter containing lignin and cellulose structures are extremely stable, making their removal from environmental samples difficult without resorting to chemically harsh procedures that would also damage plastic particles (Löder et al. 2017). However, specific types of fungi are capable of degrading lignocellulosic structures. Ramos et al. (2016) explored the in vitro production of plant cell wall–degrading enzymes by *Macrophomina phaseolina* (a fungal plant pathogen). They established, that a sequence of pectinases followed by hemicellulases and cellulases "promote initial tissue maceration followed by cell wall degradation" (Ramos et al. 2016). To emulate the fungal plant degradation, commercially available technical enzymes were used: pectinase degrades pectin, which can be found in the primary cell walls of all land plants as well as in the middle lamellae between cell walls (Willats et al. 2001). In our protocol we use 5 mL of Pektinase L-40 (polygalacturonase, pectin depolymerase, EC

TABLE 1: Enzymatic-oxidative digestion protocol for soil samples[a]

Step	Volume	Reagents	Incubation time	Incubation temperature
a	50 mL	10% sodium dodecyl sulfate	48 h	50 °C
b	50 mL	Fenton's reagent	1 h	40 °C
c	25 + 5 mL	Tris HCl 0.1 M buffer, pH 9,protease	12 h	50 °C
d	25 + 5 mL	NaAc 0.1 M buffer, pH 5,pectinase	48 h	50 °C
e	25 + 1 mL	NaAc 0.1 M buffer, pH 5, viscozyme L	48 h	50 °C
f	25 + 5 mL	NaAc 0.1 M buffer, pH 5,cellulase	24 h	40 °C
g	50 mL	Fenton's reagent	1 h	40 °C

[a]This protocol enables the removal of soil organic matter and cellulosic plant residue.

3.2.1.15; ASA Spezialenzyme) in 25 mL of 0.1 M NaAc buffer set to pH 5 with concentrated acetic acid and incubated for 48 h at 50 °C.

Step e. Viscozyme L (endo-beta-glucanase, V2010; Novozymes) is a cellulolytic enzyme mix extracted from *Aspergillus aculeatus*, with the key enzyme being endo-1,3(4)-beta glucanase, splitting the β-(1,3) linkages of the molecules. The product also contains activity of arabanase, xylanase, cellulase, and hemicellulose. Viscozyme L (1 mL) is added to the sample with 25 mL of 0.1 M NaAc buffer set to pH 5 and incubated at 50 °C for 48 h.

Step f. Cellulase TXL (endo-1,4-beta-glucanase, EC3.2.1.4; ASA Spezialenzyme) is a very similar cellulolytic enzymatic mix (cellulase, hemicellulase, xylanase) extracted from *Trichoderma longibrachiatum*, splitting the β-(1,4) linkages of the molecules. Cellulase TXL (5 mL) is added to the samples with 25 mL of 0.1 M NaAc buffer set to pH 5 and incubated at 50 °C for 24 h.

Step g. A second Fenton's reagent step is conducted, as described in step b, to remove any residual organic matter.

Second density separation. After the second Fenton's reagent step, the sample is filtered with 10-µm stainless steel filters and washed clean of any residual H_2O_2. The sample (filter cake) is then washed off the filter with a 1.8 g cm^{-3} $ZnCl_2$ solution into a precleaned glass beaker, using a stainless steel spatula to ensure the complete transfer of particles. The filter is then checked under a stereomicroscope to verify that no particles remain on the filter surface and then discarded. The $ZnCl_2$ solution–sample mixture is then transferred into a small, straight-walled separation funnel with a volume capacity of approximately 400 mL and stirred with a glass rod, which is then rinsed back into the separation funnel with $ZnCl_2$ solution to ensure that no particles are extracted accidentally. After stirring, the separation funnels are immediately covered with a glass lid and left to settle overnight (at least 12 h). This step is necessary to remove any silt or clay particles that were not removed in the first density separation step. The sediment is then released from the separation funnel and discarded, whereas the upper lightweight fraction containing floating microplastic particles is filtered onto a 10-µm stainless steel mesh filter. This is then rinsed with 98% ethanol and deionized water to remove residual $ZnCl_2$.

Transfer to sample carrier. The filter is taken out and rinsed off thoroughly with deionized water into a small glass beaker and transferred, with a small custom-made glass funnel (Ø = 10 mm), onto one or more aluminum oxide filters (0.2 µm, Anodisc; Whatman GE Healthcare), depending on the amount of particulate content in the purified sample. In this context it is important to avoid thicker layers of material because overlapping particles will obstruct the proper identification of microplastic particles in the sample.

µ-FTIR spectroscopy. The aluminum oxide filters are then measured using a Bruker Hyperion 3000 FTIR microscope (Bruker Optik), equipped with a 64 × 64-pixel FPA detector in conjunction with a Tensor 27 spectrometer. The samples are measured in transmission mode with a 3.8 × infrared objective (spatial resolution 11.05 µm) and a wavelength range of 3600 to 1250 cm^{-1} with a resolution of 8 cm^{-1} and a coaddition of 6 scans. Data processing is conducted using the Bruker OPUS software, Ver 7.5 (Bruker Optik).

Polymer classification. Automated spectral analysis is performed with the "BayreuthParticleFinder" module in ImageLab, Ver 4.1 (EPINA). This software tool allows a fast and reliable automated identification of currently 22 common plastic polymers based on the principle of random decision forest classifiers (Hufnagl et al. 2019). Alternatively, other spectroscopic analysis tools, such as the free software siMPle (Primpke et al. 2020), may be used. In principle, the purified samples may also be analyzed using Raman microspectroscopy, which potentially would allow a pixel resolution of down to 500 nm (Käppler et al. 2015). In this case smaller mesh sizes of the filters used during the whole density separation and purification procedure would be necessary.

Determination of purification efficiency

Purification efficiency was determined by gravimetric analysis. A sample of approximately 2 kg silt loam obtained from the first 10 cm of an experimental agricultural field near Stuttgart, southwest Germany, was thoroughly mixed in an aluminum pan with a spoon and then freeze-dried. Three subsamples of 250 g each were taken by the cone-and-quarter method and underwent the density separation procedure described in the section *Density separation for particles <500 µm*. Before filtering the supernatant containing the lightweight fraction, the 10-µm stainless steel mesh filters were oven-dried at 105 °C and weighed with a laboratory precision scale (d = 0.01 mg, OHAUS Explorer), with the respective weights noted. The filtered lightweight fraction was then oven-dried on the filter at 40 °C for approximately 48 h and weighed until mass consistency (±0.2 mg). The previously determined weight of the filters was subtracted to obtain the mass of the lightweight fraction.

After undergoing the enzymatic-oxidative digestion protocol as well as the second density separation step (see sections *Enzymatic-oxidative digestion* and *Second density separation*), the purified sample was again transferred onto the same stainless steel filter and washed off thoroughly with 98% ethanol and water to remove any residual $ZnCl_2$. The purified sample and filter were then dried at 40 °C and weighed until mass consistency. The mass difference of the sample matter before and after treatment was recorded and the mean purification efficiency calculated. In addition, the organic matter reduction after each purification step was photo-documented (see Figure 2) using a stereomicroscope (Leica M50; Leica

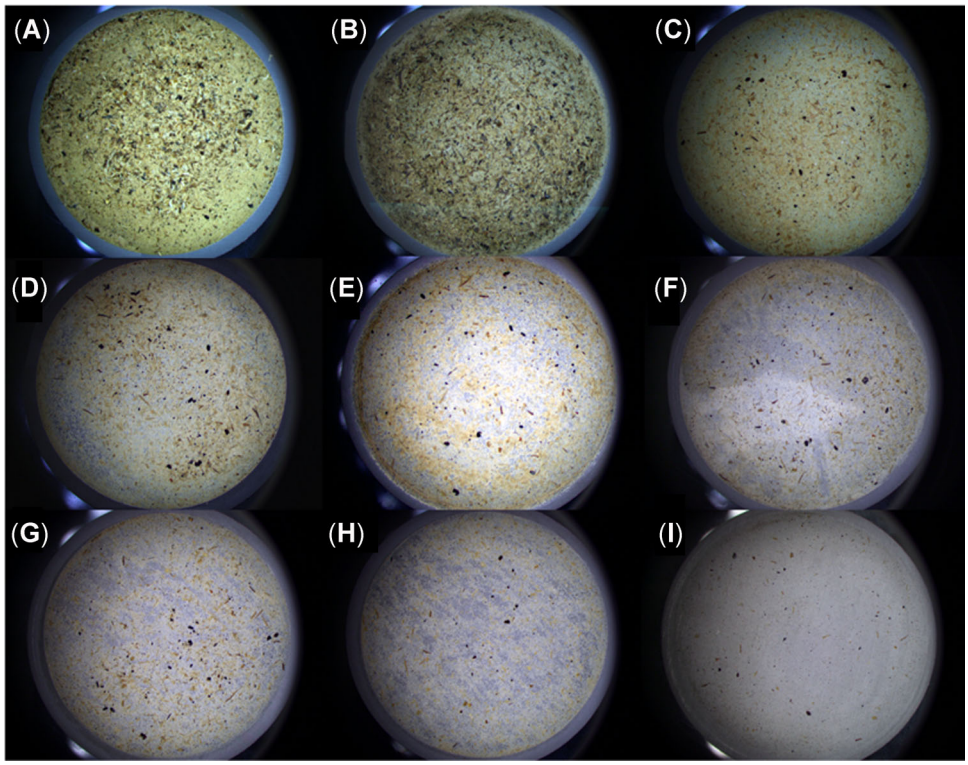

FIGURE 2: Sequential organic matter removal in the course of enzymatic-oxidative digestion—sample 3. Visual documentation of the removal efficiency of the single steps in the purification protocol. (**A**) Organic matter after density separation. (**B**) After 48-h sodium dodecyl sulfate. (**C**) After 1-h Fenton's reagent. (**D**) After 12-h protease. (**E**) After 48-h pectinase. (**F**) After 48-h viscozyme L. (**G**) After 24-h cellulase. (**H**) After 1-h Fenton's reagent. (**I**) After 24-h density separation in zinc chloride solution.

Microsystems; Olympus DP 26 camera; Olympus) and the imaging software cellSens (Olympus).

Determination of effects of the enzymatic-oxidative digestion procedure on microplastic particles

Seven different microplastic particle types were chosen to assess if the enzymatic-oxidative digestion protocol causes any damage on a visible or molecular level. Next to polymer types commonly found in environmental samples, such as the chemically resistant PE as well as polymers more vulnerable to chemical degradation such as PA, PET, and PVC, the biodegradable PLA was also tested. Polylactic acid is an increasingly popular plastic material used, for example, in 3D printing, food packaging, and bin liners for organic waste. Thus, PLA may also be among the synthetic polymers found in soils, especially agricultural soils amended with compost derived from biowaste-treatment plants.

The PLA fragments (Ø = 200 µm–1 mm) were obtained by cryo-milling virgin PLA pellets (Ingeo Biopolymer 7001D; Nature Works) and sieving the ground product. The milling and sieving were conducted by the Institute for Plastics Technology in Stuttgart. The fragments of PA (Ø = 150–300 µm, Schaetti fix 5230) and PE (Ø = 100–400 µm, Schaetti fix 140) were obtained from Schaetti. The fragments of PET (Ø = 200–400 µm) and PVC (Ø = 150–200 µm) were obtained by cryo-milling and sieving virgin pellets at the University of Bayreuth. Green fluorescent PE beads (Ø = 150–180 µm, UVPMS-BG-1.00) were obtained from Cospheric, and yellow fluorescent PET fibers (Ø = 16 µm, l = 1 mm) were obtained from a high-visibility raincoat and cut to a length of 1 mm using a pair of microscissors.

Using needle and fine-point high-precision forceps, 25 particles of each microplastic type were counted out, photographed, and fixed on a gelatin platelet (1 × 1 cm) cut from a sheet of gelatine leaf (Dr. Oetker Blatt Gelatine) under a stereomicroscope (Leica M50) equipped with an Olympus DP 26 camera. The gelatin is used to ensure that all particles can be transferred from under the stereomicroscope into the reaction containers without losing them (e.g., from static forces). The gelatin was then dissolved in water at 40 °C and filtered off, with the particles remaining on the 10-µm stainless steel mesh filter. All particles then underwent the complete enzymatic-oxidative digestion protocol including the second $ZnCl_2$ solution treatment.

Visual analysis

After every step, once the reagents were filtered off, the filter containing the microplastic particles was carefully laid under the stereomicroscope and screened for the microplastic particles, which were then photographed. Despite rinsing the filtration funnels thoroughly with water in an attempt to transfer

any adhering particles onto the filter, some particles stuck to the bottom of the funnel when extracting the filter; these particles were then directly washed back into the reaction jar with the subsequent reagent and were not photographed at the respective point in time. After the final step ($ZnCl_2$ solution), all particles were extracted from the filter with a needle and photographed without the filter as background to better compare the particles' appearance before and after the treatments. Because of static forces causing the particles to "jump," some particles were lost during transfer with the needle. The extracted particles were then kept safe for later μ-FTIR and ATR-FTIR analyses.

ATR-FTIR analysis

Because the quality of the μ-FTIR spectra in transmittance mode is dependent on the particle shape and size (e.g., very thick particles may result in the total absorption of the infrared radiation, whereas spherical particles and fibers often show disrupted spectra as a result of radiation scattering), ATR-FTIR spectroscopy was chosen as a method to compare pristine particles and the particles that underwent the enzymatic-oxidative digestion protocol. For each polymer type, respectively, 5 of the particles that underwent the enzymatic-oxidative digestion protocol were selected randomly and measured via ATR-FTIR spectroscopy (Alpha ATR-FTIR equipped with diamond crystal; Bruker Optik). For the measurement of each particle, 8 background scans were pooled, followed by 8 sample scans with a spectral resolution of 8 cm^{-1} in a wavenumber range of 4000 to 400 cm^{-1}. Using the software OPUS 7.5, the resulting spectra were compared to the spectra of untreated control particles, to determine if any changes to the functional groups in the polymer had occurred.

GPC analysis

To determine changes in the molar mass distribution of the pristine particles and particles that underwent the purification treatment, a GPC analysis was conducted.

For PLA, the GPC measurement was performed on an instrument with 4 styrene divinylbenzene (SDV) gel columns (particle size = 5 μm) with porosity range from 10^2 to 10^5 Å (Polymer Standards Service GmbH [PSS]) together with a refractive index detector (1200 Series, Agilent). Tetrahydrofuran (HPLC grade) was used as a solvent (for dissolving the polymer and as an eluting solvent) with a flow rate of 1.0 mL min^{-1}. As internal standard toluene (HPLC grade) was used. The calibration was done with narrowly distributed polystyrene (PS) homopolymers (PSS calibration kit). An injection volume of 20 μL was used for the measurements. The sample was dissolved in tetrahydrofuran and filtered through a 0.22-μm PTFE filter before analysis.

The molar mass of the rest of the polymers with the exception of PE was measured using hexafluoroisopropanol (HFIP; HPLC grade) as the eluting solvent. The GPC measurement was performed on an instrument with a perfluorinated gel (PFG) precolumn and 2 PSS-PFG columns (particle size = 7 μm) with porosity range from 100 to 300 Å (PSS) together with a refractive index detector (Agilent 1200 Series). Hexafluoroisopropanol with potassium trifluoroacetate (4.8 g in 600 mL HFIP) was used as a solvent (to dissolve the polymer and as an eluting solvent) with a flow rate of 0.5 mL min^{-1}. As an internal standard, toluene (HPLC grade) was used. The calibration was done with narrowly distributed polymethyl methacrylate (PMMA) homopolymers (PSS calibration kit). The sample was dissolved in HFIP with potassium trifluoroacetate and filtered through a 0.22-μm PTFE filter before analysis. An injection volume of 20 μL was used for the measurement, and the GPC columns were maintained at room temperature. The molar masses reported are in reference to PMMA standards.

The average mass of PE can only be analyzed by high-temperature GPC and could therefore not be analyzed in the scope of the present study.

DSC analysis

The DSC measurements were carried out on NETZSCH DSC 204F1 Phoenix instrument under a nitrogen atmosphere with a gas flow rate of 20 mL min^{-1}. A sample size of approximately 5 mg was used for each measurement. The samples were heated with a heating rate of 10 K min^{-1}.

The degree of crystallinity was calculated using the following formula:

$$Xc = \frac{\Delta Hm - \Delta Hc}{\Delta Hm^0} 100\%$$

In this equation, ΔHm is the enthalpy of melting, ΔHc is the enthalpy of crystallization, and ΔHm^0 is the enthalpy of melting for 100% crystalline polymer. Values for the enthalpy of melting for 100% crystalline PLA, low-density PE, and PET were taken as 93.6 J g^{-1} (Turner et al. 2004), 293 J g^{-1} (Atkinson and Richardson 1969), and 130 J g^{-1} (Müller et al. 2005), respectively. The actual chemical structure of PA is not known. Therefore, the percentage of crystallinity was not calculated.

RESULTS

Purification efficiency

The vast majority of the soil mass is already removed in the density separation step: of a 250-g soil sample, 52, 38, and 160 mg solid particulate matter (>10 μm) remained in the supernatant phase of the $ZnCl_2$ solution for samples 1, 2, and 3, respectively. Thus, the removal of the mineral fraction results in a mass removal of >99.9%. Nevertheless, the low-density fraction remaining in the supernatant still contains too much matter for a comprehensive μ-FTIR analysis. For the sake of simplicity, the particulate matter extracted from the supernatant will henceforth be described as the "lightweight fraction."

After the lightweight fraction was extracted, dried, and weighed, it underwent the digestion protocol, as described in the sections *Enzymatic-oxidative digestion* and *Second density*

separation. As can be seen in Figure 2, each digestion step contributes slightly to the overall high purification efficiency. Figure 2A shows the lightweight fraction collected on a 10-µm stainless steel mesh filter (Ø = 47 mm) after undergoing density separation. Although the SDS step (Figure 2B) only shows a slight discoloration of the material, the subsequent step with Fenton's reagent already shows a visible decrease of organic matter (Figure 2C). The enzymes protease, pectinase, viscozyme, and cellulase (Figure 2D–G) show a slight but significant reduction in the mostly plant-derived organic matter, which is almost completely removed by the second Fenton's reagent step (Figure 2H). The small granular structures visible in Figure 2H, which are most likely of mineral origin, are removed in the second density separation step, leaving a manageable amount of seeds, black carbon particles, and some plant-based fragments on the filter to be analyzed for the presence of microplastics. In terms of mass loss, the enzymatic-oxidative digestion protocol and second density separation protocol allowed a mass reduction of 73.9, 73.0, and 84.8% for samples 1, 2, and 3, respectively (see Figure 3). An average purification efficiency of 77.2 ± 6.6% (standard deviation) can be achieved for the lightweight fraction of soil samples. The mass losses in between the single steps of the enzymatic-oxidative digestion steps were not recorded.

Effects of the enzymatic-oxidative digestion procedure on microplastic particles

For investigation of any obvious destructive effects on the added microplastic particles caused by the purification protocol, the microplastic particles were photographed under a stereomicroscope before, during, and after the enzymatic-oxidative digestion protocol. The number of spiked and recovered particles as well as the number of optical matches per microplastic type are given in Table 2. Optical matches are to be understood as particles that do not show any visual differences in shape and size when comparing the photographs from before and after the enzymatic-oxidative digestion protocol (see Supplemental Data, Figure S1). With the exception of PA and PLA, the recovery rates for the investigated polymers were 88 to 96%. The reduced recovery in those polymers was most probably due to losses during the manual transfer from the filter. All of the recovered PET fibers and PET fragments were optical matches, whereas 2 of the recovered PE spheres

TABLE 2: Number of spiked particles, number of recovered particles, and number of optical matches

	No. spiked particles	Recovery after enzymatic digestion protocol	Optical matches
PET fibers	25	23	23
PET fragments	25	23	23
PE spheres	25	23	21
PVC fragments	25	24	22
PE fragments	25	22	21
PA fragments	25	10	9
PLA fragments	25	30	0

PET = polyethylene terephthalate; PE = polyethylene; PVC = polyvinylchloride; PA = polyamide; PLA = polylactic acid.

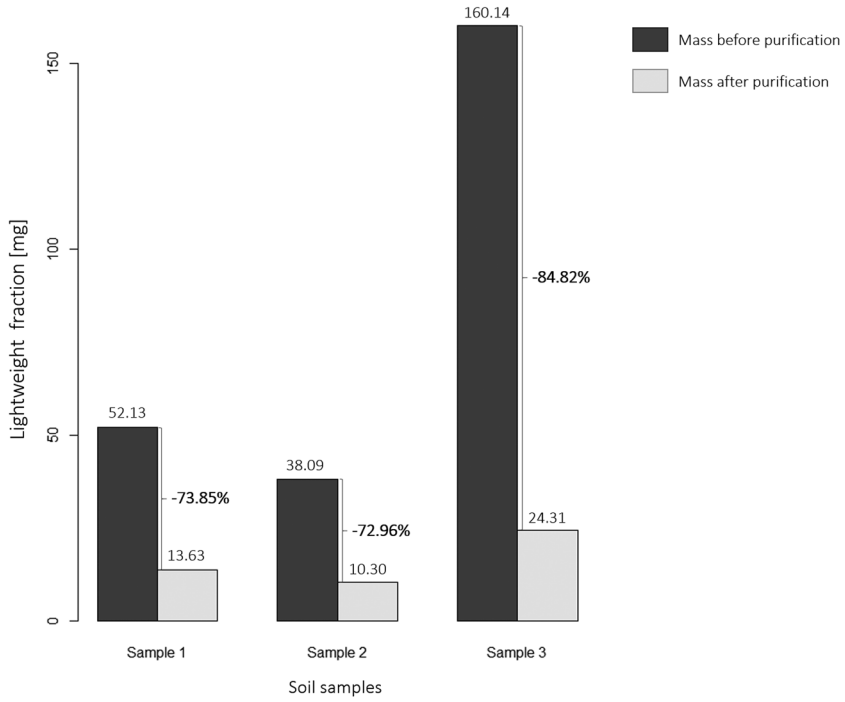

FIGURE 3: Lightweight fraction purification efficiency. The dark column represents the mass of the lightweight fraction (i.e., particulate matter remaining in the supernatant after density separation) before the enzymatic purification procedure. The light column represents the remaining mass after the purification procedure. The percentages given in bold next to the braces respectively represent the percentual mass loss.

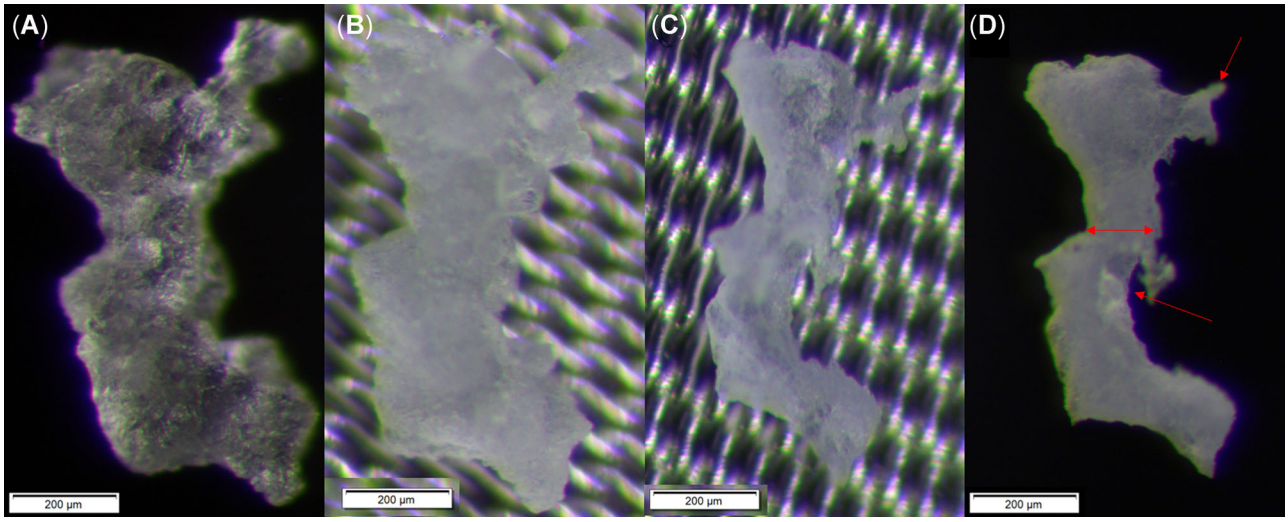

FIGURE 4: Degradation of a polylactic acid particle during the enzymatic-oxidative digestion protocol. (**A**) Particle before enzymatic-oxidative digestion protocol. (**B**) Particle after 48 h in sodium dodecyl sulfate and 1 h in Fenton's reagent. (**C**) Particle after 12-h protease. (**D**) Particle after the 5 subsequent steps (i.e., 48-h pectinase, 48-h viscozyme L, 24-h cellulase, 1-h Fenton's reagent, and 24-h $ZnCl_2$ solution).

were sharp-edged fragments, indicating that at least one of the spheres had been broken mechanically. Two of the PVC particles and one of the PE particles seemed to have become slightly smaller and rounder, possibly due to mechanical abrasion when the particles are washed against the 10-µm stainless steel mesh filter with a high-pressure water jet. Polyamide showed very low recovery rates but high optical match rates, indicating losses as a consequence of the handling and filtration steps, rather than degradation processes. One exception is PLA, where >25 particles were recovered, because of fragmentation of the particles. All PLA particles showed a notable degradation in size and shape. When comparing the particles after each step of the enzymatic-oxidative digestion protocol, it became apparent that the particles only showed signs of degradation after the 12-h protease step. The particles showed signs of surface erosion, becoming smaller and partially fragmented. No further degradation could be observed after the 5 following steps (Figure 4), indicating that the protease step was indeed the cause of the PLA particle degradation.

ATR analysis

Because of the shapes (spheres) and often relatively large thickness of the particles, ATR-FTIR analysis (instead of µ-FTIR analysis) was conducted to determine any changes in the functional groups of the particles' surface. The PET fibers, PET fragments, PE spheres, PVC fragments, low-density PE

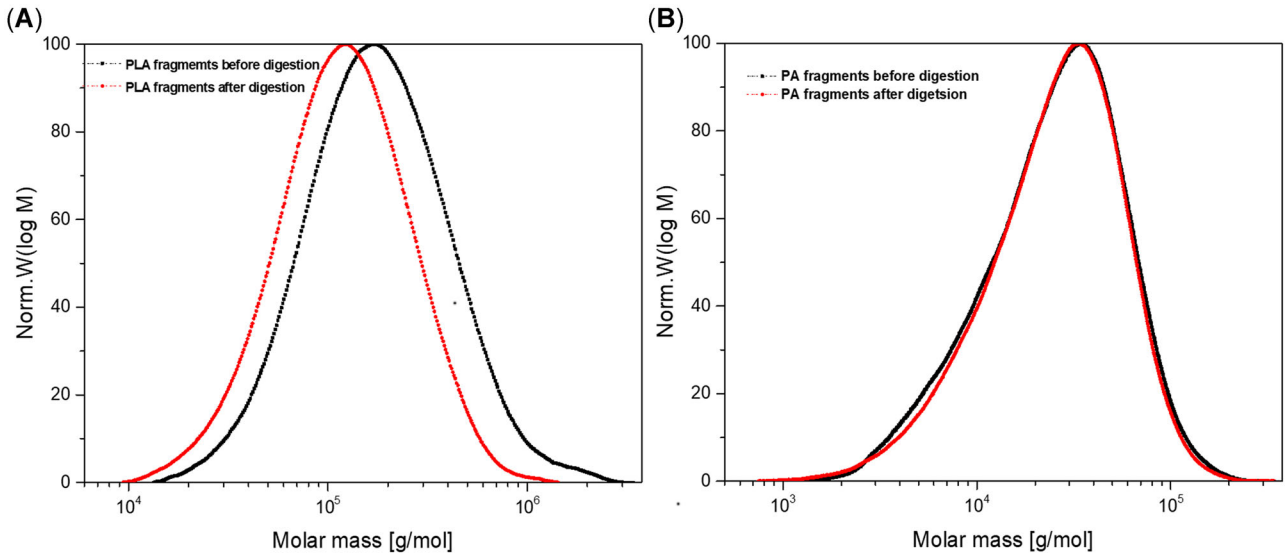

FIGURE 5: Molar mass curves of polylactic acid (**A**) and polyamide (**B**) fragments before and after digestion using hexafuoro-2-propanol eluent in gel permeation chromatography. The black curve represents the pristine polymer and the red curve, the polymer after undergoing the digestion protocol. PLA = polylactic acid; PA = polyamide; Norm. W = normalised molecular weight.

fragments, and PA fragments showed no changes in the spectral bands compared to the control particles, whereas 3 of the 5 PLA fragments showed a broad band in the region of 3300 to 3650 cm^{-1}, indicating –OH stretching, possibly as a result of degradation processes.

GPC analysis

Figure 5A shows the molar mass comparison of PLA before and after treatment, as determined by GPC using PS as the calibration standard. There was a change in the average molar mass, M_n (number average molar mass), after treatment from approximately 128.000 g mol^{-1} to approximately 89.000 g mol^{-1}, with a slight shift in molar mass dispersity from 1.93 to 1.75. The GPC curve remained unimodal. Proteolytic enzymes, such as proteases, are well known to catalyze the hydrolysis of ester bonds in aliphatic polyesters (PLA). Although, slight degradation of PLA with macromolecular chain scission was observed, PLA was not completely degraded under the conditions used in the present study based on the slow rate of hydrolysis. Other enzymes used for the treatment are not specific for polyester hydrolysis.

There was no change in the molar mass of the other polymers studied in the present study (see Figure 5B; Supplemental Data, Figures S2–S5), showing the tolerance to the steps used for sample preparation. These polymers have either a strong C–C backbone (PE, PVC) or a not easily hydrolyzable C-heteroatom backbone (PA, PET).

DSC analysis

DSC measurements were carried out to study the effect of the digestion procedure on thermal transitions of polymers. Polyvinylchloride was amorphous with a glass transition temperature (Tg) 85 ± 2 °C, which remained unchanged on digestion. Pristine PLA showed a very low degree of crystallinity (~1%). It showed a Tg of 64 ± 2 °C, broad crystallization, and melting peaks centered at 110 and 151 °C, respectively. After digestion, PLA had almost the same thermal behavior in DSC measurements concerning crystallization and melting with a degree of crystallinity of approximately 2%. The significant difference was in the enthalpy of crystallization, which was significantly higher (20.8 J g^{-1}) than that of pristine PLA (2.26 J g^{-1}). This might be due to the decrease in molar mass, as evident by GPC measurement, providing better crystallization tendency during heating. Low-density PE, PET, and PA showed semicrystalline behavior. Melting transitions were seen as broad peaks without significant change in thermal transition behavior, degree of crystallinity, and enthalpy of melting after digestion (see Supplemental Data, Figure S6 and Table S1).

Application to an environmental sample

In an exemplary 250-g subsample from the same silt-loam experimental agricultural field near Stuttgart, which was fully digested and analyzed via μ-FTIR spectroscopy, a total of 160 microplastic particles were found, of which 85% were fragments and 15% were fibers. The plastic types that were identified were, in decreasing abundance, PP (32.5%), PS (27.5%), PE (22.5%), PET (10%), polybutylene terephthalate (5%), and polyacrylonitrile (2.5%). Of the identified particles, 85% were <201 μm: 10 to 100 μm (40%), 101 to 200 μm (45%), 201 to 300 μm (10%), 301 to 400 μm (2.5%), 401 to 500 μm (2.5%; see Figure 6).

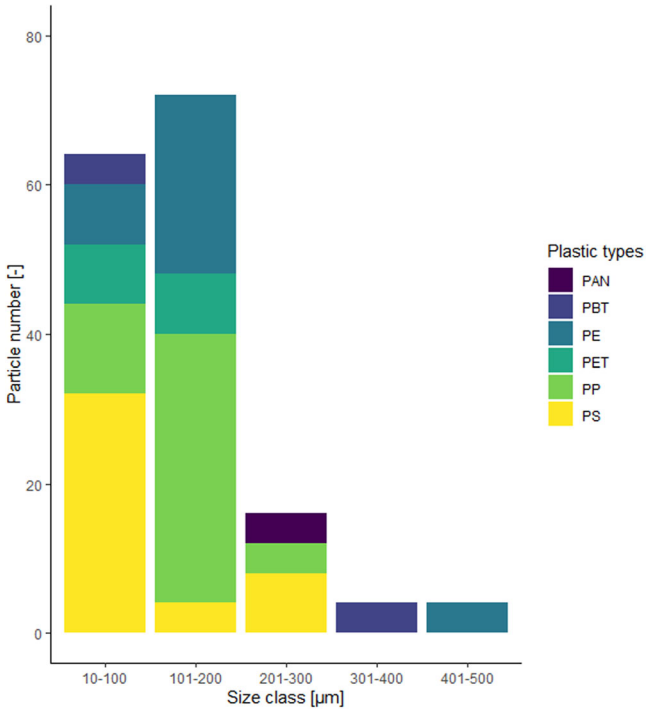

FIGURE 6: Distribution of microplastic types within different size classes in an exemplary environmental sample. PAN = polyacrylonitrile; PBT = polybutylene terephthalate; PE = polyethylene; PET = polyethylene terephthalate; PP = polypropylene; PS = polystyrene.

DISCUSSION AND CONCLUSION

The aim of the present study was to develop a soil sample purification method that 1) allows the identification microplastics in general but with a special focus on small (<500 μm) microplastic particles, 2) does not destroy conventional plastic types, and 3) enables the analysis of a relatively large sample volume of 250 g dry weight.

In this section, the differences of the soil purification protocol from previously published protocols (see Table 3) will be discussed.

Scheurer and Bigalke (2018) were among the first to publish a microplastic analysis protocol for soils that allows assessment of the size and number of microplastic particles using μ-FTIR analysis. However, the use of NaCl solution (1.2 g cm^{-3}) for density separation and hot nitric acid digestion to remove the organic matter may lead to underestimation of polymers with a density >1.2 g cm^{-3} and to an acid-induced destruction of PA, PET, and acrylonitrile butadiene styrene.

TABLE 3: Comparison between the present study and previously published purification protocols for soil samples

Reference	Density separation	Purification	Analytical method	Sample Size	Spiked MP size range	Purification efficiency	Polymer destruction/loss
Present study	$ZnCl_2$ solution (1.8 g cm^{-3}) in separation funnel	Enzymatic-oxidative digestion; duration: 8 d	ATR-FTIR and μ-FTIR spectroscopy	250 g	100–400 μm	Mineral matter >99.9%; organic matter 77.2 ± 6.6%	Destruction: PLA Tested polymers: PET, PE, PVC, PA, PLA
Scheurer and Bigalke (2018)	NaCl solution (1.2 g cm^{-3}) with centrifugation	Hot nitric acid digestion; duration: 2 d	μ-FTIR spectroscopy	50 mL	500 μm–1 mm	Mineral matter >99.9%; organic matter >99%	Destruction: ABS, PA, PET Tested polymers: PVC, PP, PE, PC, PS, PU, ABS, PA, PET
Hurley et al. (2018)	Water (1.0 g cm^{-3}) and NaI solution (1.8 g cm^{-3}) in settling tubes	Fenton's oxidation; duration: <2 h	n.a.	10 g	425 μm–1 mm	Mineral matter n.a.;organic matter 106 ± 13.8%	Destruction: none Tested polymers: PP, PE, PS, PET, PA, PC, PMMA
Han et al. (2019)	NaCl-NaI solution (1.5 g cm^{-3}) flotation	H_2O_2 (35%) oxidation; duration: 7 d	Visual sorting and ATR-FTIR spectroscopy	200 g	<1 mm	n.a.	n.d.[a]
Scopetani et al. (2020)	RO water and olive oil separation in PTFE tubes	Protocatechuic acid promoted Fenton's oxidation; duration: 1 d	ATR-FTIR and μ-FTIR spectroscopy	25 g	200 μm–2 mm	Mineral matter n.a.; organic matter 95%	Loss: PTFE[b]

[a]Nuelle et al. (2014) observed changes in PE and PP after treatment in 35% H_2O_2 for 7 d.
[b]Because of its inert properties, PTFE cannot be extracted by oil.
MP = microplastic particle; ATR-FTIR = attenuated total reflectance Fourier transform infrared; μ-FTIR = micro-Fourier-transform infrared spectroscopy; PLA = polylactic acid; PET = polyethylene terephthalate; PE = polyethylene; PVC = polyvinylchloride; PA = polyamide; ABS = acrylonitrile butadiene styrene; PP = polypropylene; PC = polycarbonate; PS = polystyrene; PU = polyurethane; n.a. = not available; PMMA = polymethyl methacrylate; n.d. = not determined; RO = reverse osmosis; PTFE = polytetrafluorethylene.

Han et al. (2019) later developed a flotation device, using a NaCl-NaI solution (1.5 g cm^{-3}), which can separate even high-density polymers from the mineral matrix. As a measure to reduce the organic matter, they propose oxidizing the lightweight organic matter with 35% H_2O_2 for a duration of 7 d, as described by Nuelle et al. (2014). In this context Nuelle et al. (2014) stated that PE and PP particles showed a reduction in size of approximately 10% after the long treatment with H_2O_2. This decrease in size may therefore bias any analytical results that include the assessment of microplastic size ranges and gives cause to assume that particles in the lower micrometer range may not be detected at all because they may have been dissolved completely.

By comparison, in the present study, visual analysis confirmed by the molecular assays (ATR-FTIR, GPC, and DSC analyses) showed that even relatively small particles (100–400 μm) made of PE, PVC, PET, and the relatively sensitive PA are not degraded during the applied purification protocol. Therefore, the present protocol is more suitable than other chemical digestion protocols using strong acids, strong bases, high temperatures, or long oxidation periods that may destroy common microplastic particles occurring in environmental samples (Löder et al. 2017; Hurley et al. 2018; Munno et al. 2018). Nevertheless, the biodegradable PLA particles showed signs of degradation and fragmentation after the protease digestion step, which needs to be considered when choosing a method for the desired analysis.

A possible alternative to the present protocol was devised by Hurley et al. (2018), in which they used NaI (1.8 g cm^{-3}) as a density separation medium and Fenton's reagent to remove the organic residue (removal efficiency 106 ± 13.8% by weight). At this point it is important to note that the organic matter removal efficiencies between Hurley's study and our study cannot be compared directly: whereas we measured the mass loss of the lightweight (organic) fraction before and after treatment, Hurley et al. (2018) determined the total organic matter content by loss-on-ignition (5.79 ± 0.19% of the sample mass) and assumed the mass loss after Fenton's oxidation to directly reflect the loss of organic matter. Potentially, also inorganic matter such as $CaCO_3$ can be oxidized, which may explain the >100% removal efficiency. This is important because the Fenton's oxidation procedure used in our study is similar to the one used by Hurley et al. (2018), but, as can be seen in Figure 2C, the organic matter removal was not complete and therefore might hamper μ-FTIR measurements. Nevertheless, because the method presented by Hurley et al. (2018) is time- and resource-efficient, application of their protocol is advisable as a first step. If, however, the residual organic matter is still too much to allow a spectroscopic analysis, the enzymatic-oxidative digestion protocol may be used to increase organic matter removal.

All of the above-mentioned protocols use a salt solution for separation of the mineral fraction from the lightweight fraction. High-density salt solutions using NaI or $ZnCl_2$ are expensive and hazardous, and therefore require an internal recycling process. Scopetani et al. (2020) presented an olive oil–based separation which is density-independent and relies on the oleophilic properties of most plastics. The method showed good recovery rates for PE, polyurethane (PU), PS, polycarbonate, PVC, and PET. But less oleophilic polymers, such as PTFE, will not be recovered and tests should be conducted if dirt and biofilms will change the extraction efficiency of aged polymers.

In comparison to previously published methods, our soil purification protocol is more elaborate but also allows processing of higher sample volumes and is very effective at removing stabilized soil organic matter. A current drawback of the purification protocol is the necessity of regularly filtering the samples over a vacuum filtration unit. This can be time- and labor-consuming and may make the system susceptible to losses and/or contamination. However, this could be avoided by applying capsuled methods like the single-pot method described by Scircle et al. (2020). The costs for each 250-g sample are, on average, 2.11 euros for the reagents of the enzymatic-oxidative digestion (see Supplemental Data, Table S2; not including costs for laboratory equipment and $ZnCl_2$ solution, which is internally regenerated and reused).

In conclusion, the present soil purification protocol has a high purification efficiency without affecting the commonly tested polymer types but does affect the biodegradable PLA. Experiments with an environmental soil sample have shown that a wide range of polymers in the shapes of fibers and fragments down to a minimum size of 10 μm can be identified with the presented method. Identifying the abundance, types, shapes, and sizes of the microplastic pollution is important for any microplastic-related risk assessment because these are relevant parameters for changes in the soil's biophysical properties as well as for the potential uptake of microplastics by soil-dwelling organisms (Wang et al. 2019). To fill the knowledge gap on the actual extent of microplastic pollution in soils, this purification protocol in combination with an automated μ-FTIR analysis could be an asset in future microplastic-monitoring schemes relying on a qualitative and quantitative microplastic assessment.

Supplemental Data—The Supplemental Data are available on the Wiley Online Library at https://doi.org/10.1002/etc.5024.

Acknowledgment—The authors especially thank the colleagues of the Department of Animal Ecology I and the Department of Macromolecular Chemistry II, with special thanks to A. Kumar, for their support in the revision and completion of the present study. The present study was conducted with the support of the Ministry for Environment, Climate Protection and Energy of Baden Württemberg, funding J.N. Möller in the scope of the German research program MiKoBo (Mikrokunststoffe in Komposten und Gärprodukten aus Bioabfallverwertungsanlagen und deren Eintrag in landwirtschaftlich genutzte Böden—Erfassen, Bewerten, Vermeiden; BWMK18007). Furthermore, the authors gratefully acknowledge the support of the German Research Foundation (391977956-SFB 1357) and the Federal Ministry of Education and Research (03F0789A) for funding the microplastic research projects "SFB Mikroplastik" and "PLAWES,"

respectively. The authors also acknowledge the support of the Institute for Plastics Technology for supplying the reference PLA fragments.

Author Contributions Statement—Study conception and design: J.N. Möller, S.D.J. Oster, S. Agarwal, M.G.J. Löder, and C. Laforsch conceived and designed the study; J.N. Möller, I. Heisel, A. Satzger, S. Agarwal, and E.C. Vizsolyi acquired the data; J.N. Möller, S. Agarwal, and E.C. Vizsolyi analyzed and interpreted the data; J.N. Möller drafted the manuscript; and J.N. Möller, I. Heisel, A. Satzger, S.D.J. Oster, S. Agarwal, M.G.J. Löder, C. Laforsch, and E.C. Vizsolyi critically revised the manuscript.

Data Availability Statement—Data, associated metadata, and calculation tools are available from the corresponding authors (julia.moeller@uni-bayreuth.de, christian.laforsch@uni-bayreuth.de, martin.loeder@uni-bayreuth.de).

REFERENCES

Atkinson CML, Richardson MJ. 1969. Thermodynamic properties of ideally crystalline polyethylene. *Transactions of the Faraday Society* 65:1764–1773.

Ciccolini LAS, Shamlou PA, Ward JM, Dunnill P. 1998. Time course of SDS–alkaline lysis of recombinant bacterial cells for plasmid release. *Biotechnol Bioeng* 60:3–5.

Corradini F, Meza P, Eguiluz R, Casado F, Huerta-Lwanga E, Geissen V. 2019. Evidence of microplastic accumulation in agricultural soils from sewage sludge disposal. *Sci Total Environ* 671:411–420.

De Souza Machado AA, Lau CW, Kloas W, Bergmann J, Bachelier- JB, Faltin E, Becker R, Görlich AS, Rillig MC. 2019. Microplastics can change soil properties and affect plant performance. *Environ Sci Technol* 53:6044–6052.

Dümichen E, Eisentraut P, Bannick CG, Barthel AK, Senz R, Braun U. 2017. Fast identification of microplastics in complex environmental samples by a thermal degradation method. *Chemosphere* 174:572–584.

Fuller S, Gautam A. 2016. A procedure for measuring microplastics using pressurized fluid extraction. *Environ Sci Technol* 50:5774–5780.

Han X, Lu X, Vogt RD. 2019. An optimized density-based approach for extracting microplastics from soil and sediment samples. *Environ Pollut* 254:113009.

He D, Luo Y, Lu S, Liu M, Song Y, Lei L. 2018. Microplastics in soils: Analytical methods, pollution characteristics and ecological risks. *Trends Analyt Chem* 109:163–172.

Huerta Lwanga E, Mendoza Vega J, Ku Quej V, Chi J de los A, Sanchez del Cid L, Chi C, Escalona Segura G, Gertsen H, Salánki T, van der Ploeg M, Koelmans AA, Geissen V. 2017. Field evidence for transfer of plastic debris along a terrestrial food chain. *Sci Rep* 7:14071.

Hufnagl B, Steiner D, Renner E, Löder MGJ, Laforsch C, Lohninger H. 2019. A methodology for the fast identification and monitoring of microplastics in environmental samples using random decision forest classifiers. *Analytical Methods* 11:2277–2285.

Hurley RR, Lusher AL, Olsen M, Nizzetto L. 2018. Validation of a method for extracting microplastics from complex, organic-rich, environmental matrices. *Environ Sci Technol* 52:7409–7417.

Hurley RR, Nizzetto L. 2018. Fate and occurrence of micro(nano)plastics in soils: Knowledge gaps and possible risks. *Curr Opin Environ Sci Health* 1:6–11.

Imhof HK, Schmid J, Niessner R, Ivleva NP, Laforsch C. 2012. A novel, highly efficient method for the separation and quantification of plastic particles in sediments of aquatic environments. *Limnol Oceanogr Methods* 10:524–537.

Käppler A, Windrich F, Löder MGJ, Malanin M, Fischer D, Labrenz M, Eichhorn K, Voit B. 2015. Identification of microplastics by FTIR and Raman microscopy: A novel silicon filter substrate opens the important spectral range below 1300 cm^{-1} for FTIR transmission measurements. *Anal Bioanal Chem* 407:6791–6801.

Kawecki D, Nowack B. 2019. Polymer-specific modeling of the environmental emissions of seven commodity plastics as macro- and microplastics. *Environ Sci Technol* 53:9664–9676.

Kumar VBN, Löschel LA, Imhof HK, Löder MGJ, Laforsch C. 2021. Analysis of microplastics of a broad size range in commercially important mussels by combining FTIR and Raman spectroscopy approaches. *Environ Pollut* 269:116147.

Lebreton L, Andrady A. 2019. Future scenarios of global plastic waste generation and disposal. *Palgrave Commun* 5:6.

Löder MGJ, Imhof HK, Ladehoff M, Löschel LA, Lorenz C, Mintenig S, Piehl S, Primpke S, Schrank I, Laforsch C, Gerdts G. 2017. Enzymatic purification of microplastics in environmental samples. *Environ Sci Technol* 51:14283–14292.

Löder MGJ, Kuczera M, Mintening S, Lorenz C, Gerdts G. 2015. Focal plane array detector-based micro-Fourier-transform infrared imaging for the analysis of microplastics in environmental samples. *Environ Chem* 12:563–581.

Maes T, Jessop R, Wellner N, Haupt K, Mayes AG. 2017. A rapid-screening approach to detect and quantify microplastics based on fluorescent tagging with Nile red. *Sci Rep* 7:44501.

Möller JN, Löder MGJ, Laforsch C. 2020. Finding microplastics in soils: A review of analytical methods. *Environ Sci Technol* 54: 2078–2090.

Müller RJ, Schrader H, Profe J, Dresler K, Deckwer WD. 2005. Enzymatic degradation of poly(ethylene terephthalate): Rapid hydrolyse using a hydrolase from *T. fusca*. *Macromol Rapid Commun* 26:1400–1405.

Munno K, Helm PA, Jackson DA, Rochman C, Sims A. 2018. Impacts of temperature and selected chemical digestion methods on microplastic particles. *Environ Toxicol Chem* 37:91–98.

Nuelle MT, Dekiff JH, Remy D, Fries E. 2014. A new analytical approach for monitoring microplastics in marine sediments. *Environ Pollut* 184:161–169.

Piehl S, Leibner A, Löder MGJ, Dris R, Bogner C, Laforsch C. 2018. Identification and quantification of macro- and microplastics on an agricultural farmland. *Sci Rep* 8:17950.

Primpke S, Cross RK, Mintenig SM, Simon M, Vianello A, Gerdts G, Vollertsen J. 2020. Toward the systematic identification of microplastics in the environment: Evaluation of a new independent software tool (siMPle) for spectroscopic analysis. *Appl Spectrosc* 74:1127–1138.

Ramos AM, Gally M, Szapiro G, Itzcovich T, Carabajal M, Levin L. 2016. In vitro growth and cell wall degrading enzyme production by Argentinean isolates of *Macrophomina phaseolina*, the causative agent of charcoal rot in corn. *Rev Argent Microbiol* 48:267–273.

Rillig MC, Ziersch L, Hempel S. 2017. Microplastic transport in soil by earthworms. *Sci Rep* 7:1362.

Rochman CM. 2018. Microplastics research—From sink to source. *Science* 360:28–29.

Scheurer M, Bigalke M. 2018. Microplastics in Swiss floodplain soils. *Environ Sci Technol* 52:3591–3598.

Schumacher BA, Shines KC, Burton JV, Papp ML. 1990. A comparison of soil homogenization techniques. In Simmons MS, ed, *Hazardous Waste Measurements*. Lewis, Chelsea, MI, USA, pp 1–40.

Scircle A, Cizdziel JV, Missling K, Li L, Vianello A. 2020. Single-pot method for the collection and preparation of natural water for microplastic analyses: Microplastics in the Mississippi River system during and after historic flooding. *Environ Toxicol Chem* 39:986–995.

Scopetani C, Chelazzi D, Mikola J, Leiniö V, Heikkinen R, Cincinelli A, Pellinen J. 2020. Olive oil–based method for the extraction, quantification and identification of microplastics in soil and compost samples. *Sci Total Environ* 733:139338.

Staricka JA, Benoit GR. 1995. Freeze-drying effects on wet and dry soil aggregate stability. *Soil Sci Soc Am J* 59:218–223.

Tagg AS, Harrison JP, Ju-Nam Y, Sapp M, Bradley EL, Sinclair CJ, Ojeda JJ. 2017. Fenton's reagent for the rapid and efficient isolation of microplastics from wastewater. *Chem Commun* 53:372–375.

Turner JF, Riga A, O'Connor A, Zhang J, Collis J. 2004. Characterization of drawn and undrawn poly-L-lactide films by differential scanning calorimetry. *J Therm Anal Calorim* 75:257–268.

Van den Berg P, Huerta-Lwanga E, Corradini F, Geissen V. 2020. Sewage sludge application as a vehicle for microplastics in eastern Spanish agricultural soils. *Environ Pollut* 261:114198.

Wang J, Liu X, Li Y, Powell T, Wang X, Wang G, Zhang P. 2019. Microplastics as contaminants in the soil environment: A mini-review. *Sci Total Environ* 691:848–857.

Weithmann N, Möller JN, Löder MGJ, Piehl S, Laforsch C, Freitag R. 2018. Organic fertilizer as a vehicle for the entry of microplastic into the environment. *Sci Adv* 4:eaap8060.

Willats WGT, Mccartney L, Mackie W, Knox JP. 2001. Pectin: Cell biology and prospects for functional analysis. *Plant Mol Biol* 47:9–27.

Zhou B, Wang J, Zhang H, Shi H, Fei Y, Huang S, Tong Y, Wen D, Luo Y, Barceló D. 2019. Microplastics in agricultural soils on the coastal plain of Hangzhou Bay, east China: Multiple sources other than plastic mulching film. *J Hazard Mater* 388:121814.

